The adjoint method in seismology – II. Applications: traveltimes and sensitivity functionals

A. Fichtner *, H.-P. Bunge, H. Igel,

Department of Earth and Environmental Sciences,
Ludwig-Maximilians University Munich, Theresienstrasse 41, D-80333 Munich, Germany

Abstract

Sensitivity functionals which allow us to express the total derivative of a physical observable with respect to the model parameters, are defined on the basis of the adjoint method. The definition relies on the existence of Green's functions for both the original and the adjoint problem. Using the acoustic wave equation in a homogeneous and unbounded medium, it is shown that the first derivative of the wavefield u with respect to the model parameter $p = c^{-2}$ (c is the wave speed) does not contain traveltime information. This property translates to any objective function defined on u and in particular to the least squares objective function. Therefore, a waveform inversion should either be complemented by a traveltime tomography or work with initially very long wavelengths that decrease in the course of the iteration. The definition of the sensitivity functionals naturally introduces waveform sensitivity kernels. Analytic examples are shown for the case of an isotropic, elastic and unbounded medium. In the case of a double couple source there are three classes of sensitivity kernels, one for each of the parameters λ, μ (Lamé parameters) and ρ (density). They decompose into P→P, P→S, S→P and S→S kernels and can be described by third-order tensors incorporating the radiation patterns of the original wavefield and the adjoint wavefield. An analysis of the sensitivity kernels for density suggests that a waveform inversion procedure should exclude either the direct waves or the source and receiver regions. S-wave sensitivity kernels, corresponding to conversions from or to S-waves, are larger than the kernels corresponding to P-waves only. This implies that S-wave residuals caused by parameter differences between the true Earth model and the numerical model will dominate a waveform inversion that does not account for that effect.

Key words: Inversion, Fréchet derivative, waveform analysis, sensitivity

* Corresponding author.
Email address: andreas.fichtner@geophysik.uni-muenchen.de (A. Fichtner).

1 Introduction

Seismological observations play an important role in the imaging of the Earth's interior structure. Radial models of density and seismic velocities, based primarily on the arrival times of seismic waves at the surface, were developed by Dziewonski & Anderson (1981), Kennett & Engdahl (1991) and Kennett et al. (1995). The one-dimensional models reflect the static increase of pressure and temperature with increasing depth and the associated phase transitions of mantle minerals. Moreover, they serve as reference models for maps of global three-dimensional variations of density and seismic velocities obtained on the basis of ray theory and finite mode summations (e.g. Dziewonski, 1984; Grand, 1994; Masters et al., 1996; Grand et al., 1997; Kennett & Gorbatov, 2004). Today, it is possible to simulate the propagation of seismic waves in realistic Earth models numerically (e.g. Igel et al., 1995; Komatitsch et al., 2000). This suggests that we replace ray theory and finite normal mode summations as forward models in inversion schemes by numeric solutions of the wave equation, thus, substantially increasing the amount of exploitable information.

The inversion of seismic data can be based on different concepts. In probabilistic inverse theory the solution of an inverse problem is defined as a marginal probability distribution in the model parameter space P (Tarantola, 1987). This definition is very general and elegant. However, a complete characterisation of this probability distribution usually requires us to evaluate a large number of parameter space elements $\mathbf{p} \in P$. Therefore, the probabilistic approach becomes impractical if the model space is large and if the solution of the forward problem is time-consuming. As an alternative, the solution of an inverse problem may be defined as the parameter set $\mathbf{p}_{min}$ that minimises an objective function $\mathfrak{E}(\mathbf{u}(\mathbf{p}))$ defined on the observable $\mathbf{u}(\mathbf{p})$. In symbols: $\mathbf{p}_{min} = \{\mathbf{p} \in P\,;\, \mathfrak{E}(\mathbf{u}(\mathbf{p})) = \min\}$. Possible observables are arrival times or waveforms. Typical parameters are seismic velocities and density. In the context of the minimisation approach the sensitivity plays a central role. It is defined as the first derivative of the observable $\mathbf{u}(\mathbf{p})$ with respect to its parameters $\mathbf{p}$ and is denoted by $D_p\mathbf{u}$. The sensitivity is the basis of resolution studies and minimisation algorithms. Moreover, it influences the choice of data that one wishes to include in the inversion procedure.

Often the computation of $D_p\mathbf{u}$ or $D_p\mathfrak{E}(\mathbf{u})$ by means of classical finite differencing techniques is impractical due to the large number of parameters in realistic models. A solution of this problem is the adjoint method (Tarantola, 1984, 1988). It allows us to obtain the first derivative by solving the original forward problem and its adjoint problem only once, therefore being very efficient. As a consequence of the continuously increasing computation power the adjoint method has received much attention in many geo-scientific fields, such as for example meteorology (Talagrand & Courtier, 1987), geodynamics (Bunge et. al, 2003), seismology (Crase et al., 1990; Igel et al., 1996; Tromp et al., 2005) or groundwater modelling (Sun, 1994).

For any application that employs the derivative $D_p\mathbf{u}$ it is important to know the type

of information that it contains. This is particularly true for inversion algorithms that exclusively rely on $D_p\mathfrak{E}(\mathbf{u})$ and therefore on $D_p\mathbf{u}$. Gauthier et al. (1986) used such an algorithm (the method of steepest descent) for the purpose of acoustic waveform inversion in two dimensions. They discovered that the derivative of the least squares objective function (the time integral over the squared waveform residuals) primarily contains information about where the edges of parameter perturbations are located. However, the interior of their famous 'Camembert' shaped bulk modulus perturbation could hardly be reconstructed during the inversion.

A particularly interesting aspect of the adjoint method is that it allows us to find analytic expressions for the different sensitivities (one for each parameter) in terms of Green's functions. This directly leads to the formulation of sensitivity kernels, i.e., volumetric sensitivity densities. Asymptotic approximations for such sensitivity kernels for body waves have been derived on the basis normal modes (Li & Tanimoto 1993; Li & Romanowicz 1995).

The objective of this study is the analysis of sensitivity functionals, expressing the sensitivity $D_p\mathbf{u}$ in terms of a functional that is independently linear in the source time function and the model perturbations. Based on the example of the acoustic wave equation in an unbounded and homogeneous medium, we show that the first derivative of the least squares objective function only contains information about scatterers and reflectors. Traveltime information about a signal with a given wavelength is not contained in the first derivative. A simple numerical example in two dimensions confirms this result, which has important implications for any seismological waveform inversion procedure that is founded on the gradient method alone. We find that even in the simple case of an unbounded, homogeneous, elastic medium, the waveform sensitivity kernels corresponding to density perturbations exhibit surprising complexity. Their shape depends on the source orientation, the observation direction and the type of wave considered. In contrast to numerically computed kernels the analytic kernels automatically decompose into P→P, P→S, S→P and S→S kernels, meaning that they are sensitivity densities for different types of conversions and therefore for different types of waveform residuals. The results derived from an analysis of the sensitivity kernels in such a simplified scenario yield important information concerning the types of waves that one should consider for a waveform inversion.

The long-term objective of this study is to contribute to the development of a waveform inversion procedure based on the adjoint method and applicable on continental or global scales. So far, waveform inversions applied to real data have mostly been based on simplified forward problems or relatively small parameter spaces (e.g., Cichowicz & Green 1992; Marquering et al. 1996; Zielhuis & van der Hilst 1996).

Before we proceed, we will briefly review the principal results obtained in the first of this series of two papers on the adjoint method in seismology (Fichtner et al., 2005). Let $\mathbf{u}$ be a field defined in time and space and depending on a set of parameters $\mathbf{p}$, i.e., $\mathbf{u} = \mathbf{u}(\mathbf{p}; \mathbf{x}, t)$. (In what follows, vectorial and potentially vectorial quantities are in bold face.) We assume that $\mathbf{u}$ is determined through a differential equation complemented by an adequate set of subsidiary conditions. Alternatively

and equivalently one may consider a *differential operator* $\mathbf{L}$ mapping $\mathbf{u}$ onto the right-hand side $\mathbf{h}$ of the differential equation:

$$\mathbf{L}(\mathbf{u};\mathbf{p},\mathbf{x},t) = \mathbf{h}(\mathbf{x},t)\,. \tag{1}$$

The operator $\mathbf{L}$ itself may depend on time t, space $\mathbf{x}$ and the parameter set $\mathbf{p}$. Solving the differential equation means to find an inverse of $\mathbf{L}$. It is usually an *objective function* $\mathfrak{E}(\mathbf{u},\mathbf{p})$ defined on $\mathbf{u}$ and $\mathbf{p}$, rather than $\mathbf{u}$ itself that is of interest. In seismology, $\mathfrak{E}$ may for example be a time integral over the difference between an observed wavefield $\mathbf{u}_0$ and a synthetically generated wavefield $\mathbf{u}$. Here, we shall assume that $\mathfrak{E}$ can be written as

$$\mathfrak{E}(\mathbf{u},\mathbf{p}) = \int_G \int_{t=t_0}^{t_1} f(\mathbf{u},\mathbf{p})\,d^3\mathbf{x}\,dt = \int_G \int_{t=t_0}^{t_1} 1\cdot f(\mathbf{u},\mathbf{p})\,d^3\mathbf{x}\,dt =: \langle 1, f(\mathbf{u},\mathbf{p})\rangle\,, \tag{2}$$

where G is the region of interest (e.g. the Earth) and $[t_0,t_1]$ the temporal observation interval. The function f must be specified for particular applications. Note that for reasons of greater generality the objective function $\mathfrak{E}$ is assumed to depend explicitly on both the observable and the parameters. Restricting our attention to linear operators $\mathbf{L}$, we found that the total derivative of $\mathfrak{E}$ with respect to the model parameters $\mathbf{p}$ in the direction $\mathbf{p}'$ can be expressed as

$$D_p\mathfrak{E}(\mathbf{u},\mathbf{p})(\mathbf{p}') = \langle \mathbf{p}', \partial_p f(\mathbf{u},\mathbf{p}) + \mathbf{L}^p(\mathbf{u},\boldsymbol{\psi})\rangle\,, \tag{3}$$

where $\mathbf{L}^p$ is the *parameter transpose* of $\mathbf{L}$. The *adjoint field* $s\psi$ has to satisfy the *adjoint equation*

$$\mathbf{L}^u(\psi;\mathbf{p},\mathbf{x},t) + \partial_u f = \mathbf{0}\,, \tag{4}$$

and a set of *adjoint subsidiary conditions*. The symbol $\mathbf{L}^u$ denotes the transpose of $\mathbf{L}$ with respect to the observable. For the two-dimensional scalar wave equation the operator $\mathbf{L}$ is

$$L(u;\rho,\mu,\mathbf{x},t) = \rho\partial_t^2 u - \nabla\cdot(\mu\nabla u)\,, \tag{5}$$

The symbols ρ and μ represent the density and shear modulus distributions, respectively. The corresponding adjoint equation coincides with the original wave equation (5) because there is no dissipation involved. Moreover, the spatial boundary conditions translate one-to-one from the original problem to the adjoint problem, whereas the initial conditions translate to terminal conditions. Using the adjoint wavefield ψ one can compute the derivative of the objective function $\mathfrak{E} = \langle 1, f\rangle$:

$$D_p\mathfrak{E}(u)(\mathbf{p}') = \langle \rho', \partial_\rho f - \partial_t\psi\,\partial_t u\rangle + \langle \mu', \partial_\mu f + (\nabla u)\cdot(\nabla\psi)\rangle\,, \quad \mathbf{p}' = (\rho',\mu')\,. \tag{6}$$

In the case of the elastic wave equation with attenuation the operator $\mathbf{L}$ is

$$\mathbf{L}(\mathbf{u};\boldsymbol{\Phi},\rho,\mathbf{x},t) = \rho(\mathbf{x})\partial_t^2\mathbf{u}(\mathbf{x},t) - \nabla\cdot\int_{-\infty}^{\infty}\boldsymbol{\Phi}(\mathbf{x},t-\tau):\nabla\mathbf{u}(\mathbf{x},\tau)\,d\tau\,, \tag{7}$$

with $\mathbf{\Phi}$ representing the fourth-order rate of relaxation tensor. The adjoint equation for this problem is found to be

$$\mathbf{L}^u(\boldsymbol{\psi}; \mathbf{\Phi}, \rho, \mathbf{x}, t) = \rho(\mathbf{x})\partial_t^2 \boldsymbol{\psi}(\mathbf{x}, t) - \nabla \cdot \int_{-\infty}^{\infty} \mathbf{\Phi}(\mathbf{x}, \tau - t) : \nabla \boldsymbol{\psi}(\mathbf{x}, \tau)\, d\tau\,.$$

(The sets of subsidiary conditions for both the original and the adjoint problem are omitted here for brevity.) The operator $\mathbf{L}$ is not symmetric, meaning that it is not identical with its transpose $\mathbf{L}^u$. Again, using the adjoint wavefield $\boldsymbol{\psi}$ one can obtain the derivative of $\mathfrak{E} = \langle 1, f \rangle$ with respect to the parameters $\mathbf{p}$:

$$\begin{aligned} D_{(\Phi,\rho)}\mathfrak{E}(\mathbf{u}, \mathbf{\Phi}, \rho)((\mathbf{\Phi'}, \rho')) &= D_\rho \mathfrak{E}(\mathbf{u}, \mathbf{\Phi}, \rho)(\rho') + D_\Phi \mathfrak{E}(\mathbf{u}, \mathbf{\Phi}, \rho)(\mathbf{\Phi'}) \\ &= \int_G \int_{t=t_0}^{t_1} \rho'(\mathbf{x}) \left[\partial_\rho f + \boldsymbol{\psi}(\mathbf{x}, t) \cdot \partial_t^2 \mathbf{u}(\mathbf{x}, t)\right] dt\, d^3\mathbf{x} \\ &+ \int_G \int_{t=0}^{t_1 - t_0} \mathbf{\Phi'}(\mathbf{x}, t) :: \left[\partial_\Phi f + \int_{\tau=t_0+t}^{t_1} \nabla \boldsymbol{\psi}(\mathbf{x}, \tau) \otimes \nabla \mathbf{u}(\mathbf{x}, \tau - t)\, d\tau\right] dt\, d^3\mathbf{x}\,. \end{aligned} \tag{8}$$

The symbol $\otimes$ denotes the tensor or dyadic product ($(\mathbf{a} \otimes \mathbf{b})_{ijkl} = a_{ij} b_{kl}$) and the symbol :: the quadruple scalar product ($\mathbf{A} :: \mathbf{B} = A_{ijkl} B_{ijkl}$).

2 Definition of the sensitivity functional

We define the sensitivity $\mathbf{s}$ to be the derivative of the physical observable $\mathbf{u} = \mathbf{u}(\mathbf{p}; \mathbf{x}, t)$ with respect to the model parameters $\mathbf{p}$ in the direction $\mathbf{p}'$ at some time $t = \tau_0$ and location $\mathbf{x} = \boldsymbol{\xi}_0$. In symbols:

$$\mathbf{s}(\boldsymbol{\xi}_0, \tau_0, \mathbf{p}') := D_p \mathbf{u}(\mathbf{p}; \boldsymbol{\xi}_0, \tau_0)(\mathbf{p}')\,. \tag{9}$$

The sensitivity is of particular importance when the solution of an inverse problem in the minimisation sense can be approximated with gradient methods. They rely on the derivative of the objective function $\mathfrak{E}$ with respect to the model parameters $\mathbf{p}$, which is given by

$$D_p \mathfrak{E}(\mathbf{u}, \mathbf{p})(\mathbf{p}') = \partial_u \mathfrak{E}(\mathbf{u}, \mathbf{p})(D_p \mathbf{u}) + \partial_p \mathfrak{E}(\mathbf{u}, \mathbf{p})(\mathbf{p}') = \partial_u \mathfrak{E}(\mathbf{u}, \mathbf{p})(\mathbf{s}) + \partial_p \mathfrak{E}(\mathbf{u}, \mathbf{p})(\mathbf{p}')\,. \tag{10}$$

The sensitivity $\mathbf{s}$ is the only contribution to $D_p\mathfrak{E}$ that is directly due to the change of the observable $\mathbf{u}$ arising from a perturbation of the model parameters $\mathbf{p}$.
In order to obtain an expression for $\mathbf{s}$, we choose a specific objective function $\mathfrak{E}_s$ which is equal to the $i-$component of the wavefield observed at $\mathbf{x} = \boldsymbol{\xi}_0$ and $t = \tau_0$:

$$\mathfrak{E}_s(\mathbf{u}, \mathbf{p}) = \mathfrak{E}_s(\mathbf{u}) = \mathbf{e}_i \cdot \mathbf{u}(\mathbf{p}; \boldsymbol{\xi}_0, \tau_0) = u_i(\mathbf{p}; \boldsymbol{\xi}_0, \tau_0)\,, \quad i = 1, 2 \text{ or } 3. \tag{11}$$

Then the derivative of $\mathfrak{E}_s$ equals the derivative of the $i-$th wavefield component, that is $D_p \mathfrak{E}_s(\mathbf{u})(\mathbf{p}') = D_p u_i(\mathbf{p}') = s_i$. When the parameter space P has a finite

dimension $m < \infty$ and basis vectors $\hat{\mathbf{e}}_k$, with $k = 1, ..., m$, then we find

$$D_p \mathfrak{E}_s(\mathbf{u})(\hat{\mathbf{e}}_k) = D_p u_i(\mathbf{p}; \boldsymbol{\xi}_0, \tau_0)(\hat{\mathbf{e}}_k) = \langle \hat{\mathbf{e}}_k, \mathbf{L}^p(\mathbf{u}, \boldsymbol{\psi}) \rangle = \frac{d}{dp_k} u_i(\mathbf{p}; \boldsymbol{\xi}_0, \tau_0)\,, \quad (12)$$

where p_k is the $k-$component of the element $\mathbf{p} \in P$. Thus, the total derivative of $\mathfrak{E}_s$ coincides with the $(i,k)-$ component of the parameter *Jacobian*. Our specific choice of the objective function $\mathfrak{E}_s$ implies that the generator f_s that links $\mathfrak{E}_s$ to the bilinear form $\langle\, .\,,\, .\, \rangle$ (see equation (2)) is determined through

$$f_s(\mathbf{u}, \mathbf{p}) = f_s(\mathbf{u}) = \mathbf{e}_i \cdot \mathbf{u}(\mathbf{p}; \mathbf{x}, t)\, \delta(\mathbf{x} - \boldsymbol{\xi}_0)\, \delta(t - \tau_0)\,, \quad (13)$$

Therefore the adjoint equation is

$$\mathbf{L}^u(\boldsymbol{\psi}; \mathbf{p}, \mathbf{x}, t) = -\partial_u f_s(\mathbf{x}, t) = -\mathbf{e}_i\, \delta(\mathbf{x} - \boldsymbol{\xi}_0)\, \delta(t - \tau_0)\,. \quad (14)$$

The adjoint source is restricted to a single point in time and space, namely to the observation time τ_0 and the observation point $\boldsymbol{\xi}_0$. Hence, by definition, $\boldsymbol{\psi}$ is the $i-$th Green's function of the adjoint problem multiplied by -1,

$$\boldsymbol{\psi}(\mathbf{p}; \mathbf{x}, t) = -\mathbf{g}_i^*(\mathbf{p}; \boldsymbol{\xi}_0, \tau_0; \mathbf{x}, t)\,, \quad (15)$$

and therefore

$$s_i(\boldsymbol{\xi}_0, \tau_0; h, \mathbf{p}') = -\langle \mathbf{p}', \mathbf{L}^p(\mathbf{u}, \mathbf{g}_i^*) \rangle\,. \quad (16)$$

Consequently, one can compute Jacobians if the Green's functions of the adjoint problem are known. In the case of linear equations, the outstanding property of Green's functions is that they allow us to represent any solution by means of a simple convolution with the source function $\mathbf{h}$ (equation (1)). Here we let $\mathbf{h}$ be a weighted superposition of spatial point sources with different directions and causal source time function h:

$$\mathbf{h}(\mathbf{x}, t) = \sum_{k=1}^{3} \alpha_k \mathbf{e}_k\, \delta(\mathbf{x} - \mathbf{x}_0)\, h(t - t_0)\,, \quad h(t)|_{t<0} = 0\,, \quad \alpha_k \in \mathbb{R}\,. \quad (17)$$

Then $\mathbf{u}$ is determined through

$$\mathbf{u}(\mathbf{x}, t) = \sum_{k=1}^{3} \alpha_k \int_{-\infty}^{\infty} \mathbf{g}_k(\mathbf{p}; \mathbf{x}_0, t_0; \mathbf{x}, t - \tau)\, h(\tau)\, d\tau\,. \quad (18)$$

Combining equations (16) and (18) yields

$$\begin{aligned} &s_i(\boldsymbol{\xi}_0, \tau_0; h, \mathbf{p}') \\ &= -\sum_{k=1}^{3} \alpha_k \int_{-\infty}^{\infty} \langle \mathbf{p}', \mathbf{L}^p[\mathbf{g}_k(\mathbf{p}; \mathbf{x}_0, t_0; \mathbf{x}, t - \tau), \mathbf{g}_i^*(\mathbf{p}; \boldsymbol{\xi}_0, \tau_0; \mathbf{x}, t)] \rangle\, h(\tau)\, d\tau\,. \end{aligned} \quad (19)$$

The sensitivity component s_i can be represented by a functional S_{ki} which is independently linear with respect to $\mathbf{p}'$ and h, respectively. We will call this operator

the *sensitivity functional*:

$$S_{ki}(\boldsymbol{\xi}_0, \tau_0; h, \mathbf{p}') := -\int_{-\infty}^{\infty} \langle \mathbf{p}', \mathbf{L}^p[\mathbf{g}_k(\mathbf{p}; \mathbf{x}_0, t_0; \mathbf{x}, t-\tau), \mathbf{g}_i^*(\mathbf{p}; \boldsymbol{\xi}_0, \tau_0; \mathbf{x}, t)]\rangle \, h(\tau)\, d\tau \,. \tag{20}$$

The symbol $:=$ denotes equality by definition. Thus,

$$s_i(\boldsymbol{\xi}_0, \tau_0; h, \mathbf{p}') = D_p u_i(\mathbf{p}; \boldsymbol{\xi}_0, \tau_0)(\mathbf{p}') = \sum_{k=1}^{3} \alpha_k S_{ki}(\boldsymbol{\xi}_0, \tau_0; h, \mathbf{p}') \,. \tag{21}$$

Here we considered only one receiver and one vectorial source. It is however straightforward to extend the concept of sensitivity functionals to multiple source/receiver geometries and to fields set off by a dipolar source.

3 Example: The acoustic wave equation

This section concentrates on the sensitivity functional for an acoustic wavefield in a homogeneous medium. Even though the problem is oversimplified, many of the results translate to more complex cases that include elasticity and heterogeneity.

3.1 Sensitivity functional

The acoustic wave equation for the case of small density variations is given by

$$L[u; p] = p(\mathbf{x})\, \partial_t^2 u(\mathbf{x}, t) - \Delta u(\mathbf{x}, t) = f(\mathbf{x}, t) \,, \tag{22a}$$

with $\mathbf{x} \in \mathbb{R}^3$ and $t \in [t_0, t_1] \subset \mathbb{R}$. The parameter p is the squared inverse of the phase velocity: $p = c^{-2}$. We complement equation (22a) by the regularity and initial conditions

$$\lim_{|\mathbf{x}|\to\infty} u(\mathbf{x}, t) = \lim_{|\mathbf{x}|\to\infty} \partial_t u(\mathbf{x}, t) = 0 \,, \tag{22b}$$

$$u(\mathbf{x}, t)|_{t\le t_0} = \partial_t u(\mathbf{x}, t)|_{t\le t_0} = 0 \,. \tag{22c}$$

The Green's function for equations (22) in the case of $p = const$ is

$$g(p; \mathbf{x}_0, t_0; \mathbf{x}, t) = \frac{1}{4\pi} \frac{\delta((t-t_0) - |\mathbf{x}-\mathbf{x}_0|/c)}{|\mathbf{x}-\mathbf{x}_0|} \,. \tag{23}$$

Since the acoustic wave equation operator is symmetric (e.g. Tarantola 1984), the adjoint equation for g^* is

$$p(\mathbf{x})\partial_t^2 g^*(p; \boldsymbol{\xi}_0, \tau_0; \mathbf{x}, t) - \Delta g^*(p; \boldsymbol{\xi}_0, \tau_0; \mathbf{x}, t) = \delta(\mathbf{x}-\boldsymbol{\xi}_0)\delta(t-\tau_0) \tag{24a}$$

with the subsidiary conditions

$$\lim_{|\mathbf{x}|\to\infty} g^*(p;\boldsymbol{\xi}_0,\tau_0;\mathbf{x},t) = \lim_{|\mathbf{x}|\to\infty} \partial_t g^*(p;\boldsymbol{\xi}_0,\tau_0;\mathbf{x},t) = 0\,, \tag{24b}$$

$$g^*(p;\boldsymbol{\xi}_0,\tau_0;\mathbf{x},t)|_{t\geq t_1} = \partial_t g^*(p;\boldsymbol{\xi}_0,\tau_0;\mathbf{x},t)|_{t\geq t_1} = 0\,. \tag{24c}$$

In equations (24), $\boldsymbol{\xi_0}$ is the observation point and $\tau_0 \in [t_0, t_1]$ is the observation time of the original acoustic field u. The solution of equations (24) for $p = const$ is

$$g^*(p;\boldsymbol{\xi}_0,\tau_0;\mathbf{x},t) = \frac{1}{4\pi}\frac{\delta((\tau_0 - t) - |\mathbf{x}-\boldsymbol{\xi}_0|/c)}{|\mathbf{x}-\boldsymbol{\xi}_0|}\,. \tag{25}$$

It remains to assemble the building blocks (23) and (25) to form the sensitivity functional S. The expression for the parameter transpose L^p is the same as in the two-dimensional case. Therefore, we find

$$\begin{aligned} S(\boldsymbol{\xi}_0,\tau_0;h,p') &= -\int_{-\infty}^{\infty} \langle p', L^p[g(p;\mathbf{x}_0,t_0;\mathbf{x},t-\tau), g^*(p;\boldsymbol{\xi}_0,\tau_0;\mathbf{x},t)]\rangle\, h(\tau)\,d\tau \\ &= -\int_{\tau=-\infty}^{\infty}\int_{t=t_0}^{t_1}\int_{\mathbb{R}^3} p'(\mathbf{x}) g^*(p;\boldsymbol{\xi}_0,\tau_0;\mathbf{x},t)\partial_t^2 g(p;\mathbf{x}_0,t_0;\mathbf{x},t-\tau)\,h(\tau)\,d\tau\,dt\,d^3\mathbf{x} \\ &= -\frac{1}{(4\pi)^2}\int_{t=t_0}^{t_1}\int_{\mathbb{R}^3} p'(\mathbf{x})\delta[(\tau_0 - t) - |\mathbf{x}-\boldsymbol{\xi}_0|/c]\frac{\ddot{h}(t-t_0-|\mathbf{x}-\mathbf{x}_0|/c)}{|\mathbf{x}-\boldsymbol{\xi}_0||\mathbf{x}-\mathbf{x}_0|}\,d^3\mathbf{x}\,dt. \end{aligned} \tag{26}$$

The integral over t is non-zero only if the condition

$$\tau_0 \in [t_0 + |\mathbf{x}-\boldsymbol{\xi}_0|/c\,,\ t_1 + |\mathbf{x}-\boldsymbol{\xi}_0|/c] \tag{27}$$

is satisfied. (Note that we already require $\tau_0 \in [t_0, t_1]$.) If relation (27) indeed holds, we obtain

$$S(\boldsymbol{\xi}_0,\tau_0;h,p') = -\frac{1}{(4\pi)^2}\int_{\mathbb{R}^3} p'(\mathbf{x})\frac{\ddot{h}[\tau_0 - t_0 - (|\mathbf{x}-\mathbf{x}_0| + |\mathbf{x}-\boldsymbol{\xi}_0|)/c]}{|\mathbf{x}-\boldsymbol{\xi}_0||\mathbf{x}-\mathbf{x}_0|}\,d^3\mathbf{x}\,. \tag{28}$$

This is the derivative of the displacement field of an acoustic wave in a homogeneous medium with respect to $p = c^{-2}$.

3.2 Traveltime information

Due to the causality of h the sensitivity functional is non-zero only if the relation

$$c(\tau_0 - t_0) \geq |\mathbf{x}-\mathbf{x}_0| + |\mathbf{x}-\boldsymbol{\xi}_0| \tag{29}$$

can be satisfied for some $\mathbf{x} \in \mathbb{R}$. This is possible only for $c(\tau_0 - t_0) \geq |\mathbf{x}_0 - \boldsymbol{\xi}_0|$, because $c(\tau_0 - t_0) < |\mathbf{x}_0 - \boldsymbol{\xi}_0|$ would violate the triangle inequality. Thus,

$$D_p u(p;\boldsymbol{\xi}_0,\tau_0)(p') = 0\,, \quad \forall\ \tau_0 < t_0 + |\mathbf{x}_0 - \boldsymbol{\xi}_0|/c\,. \tag{30}$$

In other words: The derivative of the acoustic wavefield u with respect to the parameter $p = c^{-2}$ in any direction p' at some observation point $\boldsymbol{\xi}_0$ is identically zero prior to the first arrival which occurs at the time $t = t_0 + |\mathbf{x}_0 - \boldsymbol{\xi}_0|/c$. Consequently, we can perturb the medium arbitrarily and $D_p u(p; \boldsymbol{\xi}_0, \tau_0)(p')$ will always be zero prior to the first arrival at $\mathbf{x} = \boldsymbol{\xi}_0$. However, we know that increasing the wavespeed somewhere between source $\mathbf{x}_0$ and receiver $\boldsymbol{\xi}_0$ will lead to earlier arrivals.
The resolution of this apparent paradox imposes significant constraints on the applicability of pure gradient methods in the field of waveform inversion. Assume that the wave field $u(p; \mathbf{x}, t)$ is sufficiently smooth with respect to p to allow its expansion into a Taylor series,

$$u(p + p'; \mathbf{x}, t) = u(p; \mathbf{x}, t) + D_p u(p; \mathbf{x}, t)(p') + \frac{1}{2} D_p^2 u(p; \mathbf{x}, t)(p', p') + ... \quad (31)$$

(Note that the perturbation $p' = p'(\mathbf{x})$ does not need to be restricted to a point. It can be spatially extended.) The unperturbed field $u(p; \mathbf{x}, t)$ and the perturbed field $u(p + p'; \mathbf{x}, t)$ are both governed by an acoustic wave equation

$$p\, \partial_t^2 u(p; \mathbf{x}, t) - \Delta u(p; \mathbf{x}, t) = \delta(\mathbf{x} - \mathbf{x}_0) h(t - t_0)\,, \quad (32)$$
$$(p + p')\, \partial_t^2 u(p + p'; \mathbf{x}, t) - \Delta\, u(p + p'; \mathbf{x}, t) = \delta(\mathbf{x} - \mathbf{x}_0) h(t - t_0)\,. \quad (33)$$

Combining equations (32) and (33) and inserting the Taylor expansion of u, we obtain, correct to first order in $||p'||$,

$$p\, \partial_t^2 D_p u(p; \mathbf{x}, t)(p') - \Delta\, D_p u(p; \mathbf{x}, t)(p') = -p' \partial_t^2 u(p; \mathbf{x}, t)\,. \quad (34)$$

Equation (34) states that correct to first order in $||p'||$ the perturbed wave field $u(p + p'; \mathbf{x}, t)$ is given by the sum of the unperturbed wave field $u(p; \mathbf{x}, t)$ and the wave field $D_p u(p; \mathbf{x}, t)(p')$. The latter is set off by secondary sources that act when the unperturbed wave field reaches the perturbation $p'(\mathbf{x})$. The time when the sources for $D_p u(p; \mathbf{x}, t)(p')$ act, is therefore independent of the actual perturbation $p'(\mathbf{x})$. Consequently, correct to first order, the wave field $D_p u(p; \mathbf{x}, t)(p')$ must arrive later at some point $\mathbf{x} = \boldsymbol{\xi}_0$ than the unperturbed field $u(p; \mathbf{x}, t)$. The first derivative of the displacement field u with respect to the model parameters only accounts for scattering caused by finite perturbations. This implies that traveltime differences must be contained in higher derivatives. Hence, one may symbolically write

$$u(p + p'; \mathbf{x}, t) - u(p; \mathbf{x}, t) = \text{scattering (1st derivative)} \\ + \text{travel time differences (higher derivatives)}\,. \quad (35)$$

Note that equation (10) states that this property also influences the derivative of any objective function $\mathfrak{E}(\mathbf{u}, \mathbf{p})$ with respect to the parameters. This phenomenon also manifests itself in a simple numerical example (see figure 1) that is based on a finite differences solution of the two-dimensional scalar wave equation

$$\rho(\mathbf{x})\, \partial_t^2 u(\mathbf{x}, t) - \nabla \cdot (\mu(\mathbf{x})\, \nabla u(\mathbf{x}, t)) = g(\mathbf{x}, t)\,, \qquad \mathbf{x} \in G \subset \mathbb{R}^2 \quad (36)$$

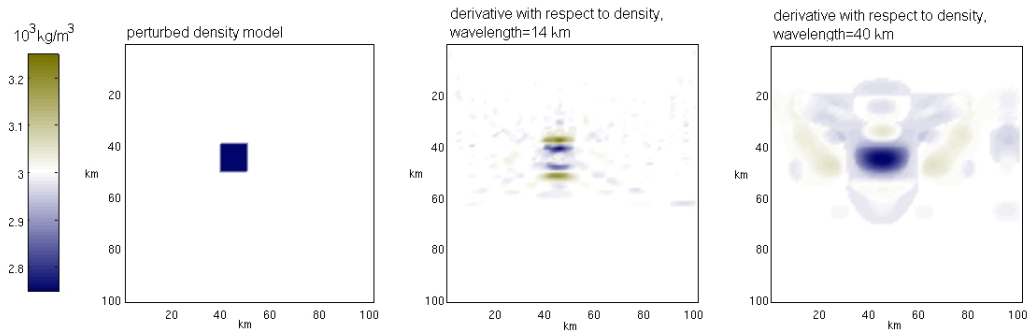

Fig. 1. **Left**: Perturbed density model. The reference model is homogeneous in both density and shear modulus ($\rho = 3.0 \cdot 10^3\,\mathrm{kg\,m^{-3}}$, $\mu = 75.0 \cdot 10^9\,\mathrm{N\,m^{-2}}$). There are no shear modulus perturbations. **Middle**: Derivative of the objective function $\mathfrak{E}$ with respect to density for a dominant signal wavelength of $\lambda_0 = 14\,\mathrm{km}$. Only the edges of the perturbation are mapped by $D_\rho \mathfrak{E}$. The interior of the density perturbation remains invisible. (The colorbar only applies to the figure on the left because the amplitude of the derivatives are proportional to the amplitudes of the signal.) **Right**: $D_\rho \mathfrak{E}$ for $\lambda_0 = 40\,\mathrm{km}$. Since the wavelength is longer, the entire density perturbation acts as a scatterer. It therefore maps as one single object into the derivative.

in a square region. The parameters ρ and μ are density and shear modulus, respectively. The upper boundary is free (no tractions), the lower boundary is rigid (no displacement) and periodic boundary conditions are implemented on the left and right boundaries. Ten receivers at a mutual distance of $10\,\mathrm{km}$ are located along the upper boundary. Their positions coincide with those of ten sources which radiate a Ricker wavelet. Homogeneous density and shear modulus distributions ($\rho = 3.0 \cdot 10^3\,\mathrm{kg\,m^{-3}}$, $\mu = 75.0 \cdot 10^9\,\mathrm{N\,m^{-2}}$) serve as references. The perturbed model contains in its centre a square box where the density is reduced to a value of $2.75 \cdot 10^3\,\mathrm{kg\,m^{-3}}$ (see figure 1, left). The shear modulus distribution $\mu(\mathbf{x})$ remains unchanged. A time integral over the sum of all squared residuals is used as objective function $\mathfrak{E}$:

$$\mathfrak{E}(u) = \frac{1}{2} \sum_{k=1}^{10} \int_{t=t_0}^{t_1} \left[u(\mathbf{x}_k, t) - u_0(\mathbf{x}_k, t)\right]^2 dt\,. \tag{37}$$

The wavefields u and u_0 correspond to the perturbed and the unperturbed models, respectively. As expected, the derivative of $\mathfrak{E}$ with respect to density depends strongly on the dominant wavelength λ_0 of the signal. Choosing $\lambda_0 = 14\,\mathrm{km}$ results in the derivative shown in the middle of figure 1. Rather than mapping the entire box, the derivative is large only along its upper and lower edges. Those parts of the perturbation act as reflectors for signals with a wavelength that is short compared to the extension of the perturbation. Since it depends on the wavelength whether a perturbation acts completely as scatterer or not, it is possible to map the entire density perturbation by choosing a longer wavelength. The derivative of $\mathfrak{E}$ with respect to density for the wavelength $\lambda_0 = 40\,\mathrm{km}$ is shown on the right of figure 1. As predicted, the density perturbation is mapped in the form of a single gradient contribution because it acts as one scatterer for this particular wave. Naturally, the gradient peak is much broader due to the longer wavelength.

A profound implication arising from the above considerations is that a waveform inversion based exclusively on the first derivative of the wavefield or any associated objective function is not well suited for the determination of structure that has a significantly longer wavelength than the signal. Consequently, the waveform inversion must either be based on a more sophisticated iterative procedure that includes higher derivatives or it must be complemented by a conventional traveltime tomography. That a waveform inversion requires a background model that explains traveltimes sufficiently well has also been found by Crase et al. (1990) and Igel et al. (1996).

4 Waveform sensitivity kernels in homogeneous isotropic media

Based on equation (20) one may approximate sensitivity functionals numerically for almost arbitrarily complex media. However, in order to gain physical understanding it is important to analyse simplified problems that can be solved analytically. In the particular case of the wave equation in a homogeneous, isotropic and unbounded medium, it is possible to demonstrate the complexities arising from wave conversions which are due to perturbations in different parameters.
Consider the operator $\mathbf{L}$ corresponding to the general wave equation (equation (7)). By inserting the time-localised and isotropic constitutive relation

$$\mathbf{\Phi}(\mathbf{x},t) = \mathbf{\Phi}^0(\mathbf{x})\delta(t)\,, \qquad \Phi^0_{ijkl} = \lambda\delta_{ij}\delta_{kl} + \mu\delta_{ik}\delta_{jl} + \mu\delta_{il}\delta_{jk}\,, \tag{38}$$

the operator $\mathbf{L}$ and its displacement transpose $\mathbf{L}^u$ reduce to

$$\mathbf{L}[\mathbf{u};\rho,\lambda,\mu,\mathbf{x},t] = \rho\partial_t^2\mathbf{u} - (2\mu+\lambda)\nabla\nabla\cdot\mathbf{u} + \mu\nabla\times(\nabla\times\mathbf{u}) \tag{39}$$

and

$$\mathbf{L}^u[\boldsymbol{\psi};\rho,\lambda,\mu,\mathbf{x},t] = \rho\partial_t^2\boldsymbol{\psi} - (2\mu+\lambda)\nabla\nabla\cdot\boldsymbol{\psi} + \mu\nabla\times(\nabla\times\boldsymbol{\psi})\,. \tag{40}$$

The Lamé parameters λ and μ are assumed constant. Since the time-localised rheology eliminates anelasticity, $\mathbf{L}$ becomes symmetric. Also based on (38), one finds that the total derivative of the least squares objective function $\mathfrak{E}$ with respect to the parameters $\mathbf{p} = (\rho,\lambda,\mu)$ and in the direction $\mathbf{p}' = (\rho',\lambda',\mu')$ simplifies to

$$\begin{aligned} D_p\mathfrak{E}(\mathbf{u})(\mathbf{p}') = &-\int_{\mathbb{R}^3}\int_{t=t_0}^{t_1}\rho'\,\partial_t\boldsymbol{\psi}\cdot\partial_t\mathbf{u}\,dt\,d^3\mathbf{x} + \int_{\mathbb{R}^3}\int_{t=t_0}^{t_1}\lambda'(\nabla\cdot\boldsymbol{\psi})(\nabla\cdot\mathbf{u})\,dt\,d^3\mathbf{x} \\ &+\int_{\mathbb{R}^3}\int_{t=t_0}^{t_1}\mu'[(\nabla\boldsymbol{\psi}):(\nabla\mathbf{u}) + (\nabla\boldsymbol{\psi}):(\nabla\mathbf{u})^T]\,dt\,d^3\mathbf{x}\,. \end{aligned} \tag{41}$$

Here it is assumed that $\mathfrak{E}$ does not explicitly depend on $\mathbf{p}$. The sources of most tectonic earthquakes can be approximated by a superposition of dipoles

$$\begin{aligned}\mathbf{f}_{pq}(\mathbf{x},t) &= (\mathbf{e}_q \cdot \nabla_{x_0})\delta(\mathbf{x}-\mathbf{x}_0)h(t-t_0)\,\mathbf{e}_p \\ &= \lim_{\varepsilon\to 0}\frac{1}{\varepsilon}[\delta(\mathbf{x}-\mathbf{x}_0+\varepsilon\mathbf{e}_q)\,\mathbf{e}_p - \delta(\mathbf{x}-\mathbf{x}_0)\,\mathbf{e}_p]\,h(t-t_0)\,, \end{aligned} \tag{42}$$

where h is a causal source time function. With $\mathbf{g}_p(\mathbf{x}_0,t_0;\mathbf{x},t)$ the Green's function for a single spatio-temporal point force acting at $\mathbf{x}=\mathbf{x}_0$ and $t=t_0$ in the direction of $\mathbf{e}_p$, the solution for the $(p,q)-$dipole $\mathbf{f}_{pq}$ is

$$\mathbf{g}_{pq}(\mathbf{x}_0,t_0;\mathbf{x},t) := (\mathbf{e}_q \cdot \nabla_{x_0})\mathbf{g}_p(\mathbf{x}_0,t_0;\mathbf{x},t)\,. \tag{43}$$

The symbol $:=$ denotes equality by definition. A general displacement field resulting from a weighted superposition of all possible dipoles can then be expressed in the form

$$\mathbf{u}(\mathbf{x},t) = \sum_{p,q=1}^{3} M_{pq}\int_{-\infty}^{\infty}\mathbf{g}_{pq}(\mathbf{x}_0,t_0;\mathbf{x},t-\tau)\,h(\tau)\,d\tau\,, \tag{44}$$

where the scalars M_{pq} are the moment tensor components. A comparison with equations (18) to (21) suggests that the appropriate definition of the sensitivity functional for the case of a dipolar source is given by the following set of equations:

$$s_n(\boldsymbol{\xi}_0,\tau_0;h,\mathbf{p}') = \sum_{p,q=1}^{3} M_{pq}S_{pqn}(\boldsymbol{\xi}_0,\tau_0;h,\mathbf{p}')\,, \tag{45a}$$

$$S_{pqn}(\boldsymbol{\xi}_0,\tau_0;h,\mathbf{p}') = S^{\rho}_{pqn}(\boldsymbol{\xi}_0,\tau_0;h,\rho') + S^{\lambda}_{pqn}(\boldsymbol{\xi}_0,\tau_0;h,\lambda') + S^{\mu}_{pqn}(\boldsymbol{\xi}_0,\tau_0;h,\mu')\,, \tag{45b}$$

$$\begin{aligned}S^{\rho}_{pqn}(\boldsymbol{\xi}_0,\tau_0;h,\rho') = \int_{-\infty}^{\infty}\int_{t=t_0}^{t_1}\int_{\mathbb{R}^3}&\rho'\partial_t\mathbf{g}_{pq}(\mathbf{x}_0,t_0;\mathbf{x},t-\tau) \\ &\cdot\partial_t\mathbf{g}^*_n(\boldsymbol{\xi}_0,\tau_0;\mathbf{x},t)\,h(\tau)\,d^3\mathbf{x}\,dt\,d\tau\,,\end{aligned} \tag{45c}$$

$$\begin{aligned}S^{\lambda}_{pqn}(\boldsymbol{\xi}_0,\tau_0;h,\lambda') = -\int_{-\infty}^{\infty}\int_{t=t_0}^{t_1}\int_{\mathbb{R}^3}&\lambda'\,[\nabla\cdot\mathbf{g}_{pq}(\mathbf{x}_0,t_0;\mathbf{x},t-\tau)] \\ &\cdot[\nabla\cdot\mathbf{g}^*_n(\boldsymbol{\xi}_0,\tau_0;\mathbf{x},t)]\;h(\tau)\,d^3\mathbf{x}\,dt\,d\tau\,,\end{aligned} \tag{45d}$$

$$\begin{aligned}S^{\mu}_{pqn}(\boldsymbol{\xi}_0,\tau_0;h,\mu') = &-\int_{-\infty}^{\infty}\int_{t=t_0}^{t_1}\int_{\mathbb{R}^3}\mu'[\nabla\mathbf{g}_{pq}(\mathbf{x}_0,t_0;\mathbf{x},t-\tau)] \\ &\qquad:[\nabla\mathbf{g}^*_n(\boldsymbol{\xi}_0,\tau_0;\mathbf{x},t)]\,h(\tau)\,d^3\mathbf{x}\,dt\,d\tau\,, \\ &-\int_{-\infty}^{\infty}\int_{t=t_0}^{t_1}\int_{\mathbb{R}^3}\mu'[\nabla\mathbf{g}_{pq}(\mathbf{x}_0,t_0;\mathbf{x},t-\tau)] \\ &\qquad:[\nabla\mathbf{g}^*_n(\boldsymbol{\xi}_0,\tau_0;\mathbf{x},t)]^T\,h(\tau)\,d^3\mathbf{x}\,dt\,d\tau\,.\end{aligned} \tag{45e}$$

Due to the simplicity of the problem it is possible to derive exact expressions for the dipole Green's functions (e.g. Aki & Richards, 2002). Restricting our considerations to the far field we may write $\mathbf{g}_{pq}$ as a sum of an S-wave and a P-wave contribution:

$$\mathbf{g}_{pq}^{PFF}(\mathbf{x}_0, t_0; \mathbf{x}, t) = \frac{\gamma_p^{(s)}\gamma_q^{(s)}}{4\pi\rho\alpha^3 r^{(s)}} \frac{\mathbf{r}^{(s)}}{r^{(s)}} \dot{\delta}\left(t - t_0 - \frac{r^{(s)}}{\alpha}\right), \tag{46a}$$

$$\mathbf{g}_{pq}^{SFF}(\mathbf{x}_0, t_0; \mathbf{x}, t) = \frac{\gamma_q^{(s)}}{4\pi\rho\beta^3 r^{(s)}} \left(\mathbf{e}_p - \frac{\mathbf{r}^{(s)}}{r^{(s)}}\gamma_p^{(s)}\right) \dot{\delta}\left(t - t_0 - \frac{r^{(s)}}{\beta}\right). \tag{46b}$$

The $P-$wave speed α and the $S-$wave speed β are $\sqrt{(2\mu+\lambda)/\rho}$ and $\sqrt{\mu/\rho}$, respectively. The distance from the source is $\mathbf{r}^{(s)} = |\mathbf{x} - \mathbf{x}_0|$ and $\gamma_i^{(s)} = r_i^{(s)}/r^{(s)}$ is the direction cosine measured from the source. The superscript XFF with $X = P$ or $X = S$ is a reminder that this is a far field approximation. As a final building block we require the adjoint Green's functions. Since the adjoint wave equation coincides with the original wave equation in the case of perfect elasticity, the adjoint Green's functions $\mathbf{g}_n^*$ are identical to the original Green's functions, the only difference being that the $\mathbf{g}_n^*$ have to satisfy the terminal conditions. Therefore we find

$$\mathbf{g}_n^{*\,PFF}(\boldsymbol{\xi}_0, \tau_0; \mathbf{x}, t) = \frac{1}{4\pi\rho\alpha^2 r^{(r)}} \frac{\mathbf{r}^{(r)}}{r^{(r)}} \gamma_n^{(r)} \delta\left(\frac{r^{(r)}}{\alpha} + t - \tau_0\right), \tag{47a}$$

$$\mathbf{g}_n^{*\,SFF}(\boldsymbol{\xi}_0, \tau_0; \mathbf{x}, t) = \frac{1}{4\pi\rho\beta^2 r^{(r)}} \left(\mathbf{e}_n - \frac{\mathbf{r}^{(r)}}{r^{(r)}}\gamma_n^{(r)}\right) \delta\left(\frac{r^{(r)}}{\beta} + t - \tau_0\right). \tag{47b}$$

with $\mathbf{r}^{(r)} = (\mathbf{x} - \boldsymbol{\xi}_0)$ and $\gamma_i^{(r)}$ the corresponding direction cosines measured from the receiver. Again, this is a far field approximation, which is justified when the parameter perturbations ρ', λ' and μ' are several wavelengths away from both source and receiver. However, if a perturbation is close to the receiver it becomes necessary to include the near field terms in the adjoint Green's functions $\mathbf{g}_n^*$. Similarly, perturbations near the source will require the near and intermediate field terms in $\mathbf{g}_{pq}$. Consequently, both the source and the receiver regions have to be excluded from the considerations in the case of the far field approximation.
In the appendix it is demonstrated that the sensitivity functional for density perturbations can be reduced to

$$\begin{aligned} S_{pqn}^{\rho}(\boldsymbol{\xi}_0, \tau_0; h, \rho') = &- \int_{\mathbb{R}^3} \mathbf{a}_{pq}^{PFF} \cdot \mathbf{b}_n^{PFF}\ \dddot{h}\left(\tau_0 - t_0 - r^{(s)}/\alpha - r^{(r)}/\alpha\right) d^3\mathbf{x} \\ &- \int_{\mathbb{R}^3} \mathbf{a}_{pq}^{PFF} \cdot \mathbf{b}_n^{SFF}\ \dddot{h}\left(\tau_0 - t_0 - r^{(s)}/\alpha - r^{(r)}/\beta\right) d^3\mathbf{x} \\ &- \int_{\mathbb{R}^3} \mathbf{a}_{pq}^{SFF} \cdot \mathbf{b}_n^{PFF}\ \dddot{h}\left(\tau_0 - t_0 - r^{(s)}/\beta - r^{(r)}/\alpha\right) d^3\mathbf{x} \\ &- \int_{\mathbb{R}^3} \mathbf{a}_{pq}^{SFF} \cdot \mathbf{b}_n^{SFF}\ \dddot{h}\left(\tau_0 - t_0 - r^{(s)}/\beta - r^{(r)}/\beta\right) d^3\mathbf{x}\,. \end{aligned} \tag{48}$$

The contributions for the volumetric sensitivity kernels $\mathbf{a}_{pq}^{XFF}$ and $\mathbf{b}_{n}^{YFF}$, where X and Y can be P or S, are given by

$$\mathbf{a}_{pq}^{PFF} = \frac{\gamma_p^{(s)}\gamma_q^{(s)}}{4\pi\rho\alpha^3 r^{(s)}}\frac{\mathbf{r}^{(s)}}{r^{(s)}}\,, \qquad \mathbf{a}_{pq}^{SFF} = \frac{\gamma_q^{(s)}}{4\pi\rho\beta^3 r^{(s)}}\left(\mathbf{e}_p - \frac{\mathbf{r}^{(s)}}{r^{(s)}}\gamma_p^{(s)}\right)\,,$$
$$\mathbf{b}_{n}^{PFF} = \frac{\gamma_n^{(r)}}{4\pi\rho\alpha^2 r^{(r)}}\frac{\mathbf{r}^{(r)}}{r^{(r)}}\,, \qquad \mathbf{b}_{n}^{SFF} = \frac{1}{4\pi\rho\beta^2 r^{(r)}}\left(\mathbf{e}_n - \frac{\mathbf{r}^{(r)}}{r^{(r)}}\gamma_n^{(r)}\right)\,. \tag{49}$$

Evidently, these factors just coincide with the radiation patterns of the original and the adjoint Green's functions, respectively. In the case of perturbations in Lamé's parameters the corresponding expressions will become more complex. Note that the causality of the source time function h implies that all sensitivity functionals for density with kernels

$$R_{pqn}^{X\to Y} := -\mathbf{a}_{pq}^{XFF}\cdot\mathbf{b}_{n}^{YFF} \tag{50}$$

are identically zero if the observation time τ_0 does not satisfy the condition

$$\tau_0 \geq t_0 + r^{(s)}/c_X + r^{(r)}/c_Y\,, \quad c_p = \alpha\,, c_s = \beta\,. \tag{51}$$

This is again a manifestation of the fact that the first derivative of $\mathfrak{E}$ and therefore the sensitivity functionals do not contain traveltime information. The observation time has to be larger than the time required for a wave in the unperturbed medium to travel from the source $\mathbf{x}_0$ to a perturbation at $\mathbf{x}$ and from there to the receiver at $\boldsymbol{\xi}_0$. The volumetric sensitivity kernels themselves are not dependent on time. However, only those regions of them are sampled where the expression

$$\dddot{h}(\tau_0 - t_0 - r^{(s)}/\beta - r^{(r)}/\beta) \tag{52}$$

is non-zero. The existence of four kernels is the consequence of possible conversions from P-waves to S-waves and vice versa.

Superpositions of two dipoles (double couples) are of particular interest in seismology. They can be used to approximate sources corresponding to slip across a fault plane. The number of possible sensitivity kernels in the case of a double couple source is 36 for each one of the parameters ρ, μ and λ. There are 3 observation directions n ($n = 1, 2, 3$), 3 distinct double couples ($(p, q) = (1, 2), (1, 3), (2, 3)$), and 4 different types of kernels (P→P, P→S, S→P, S→S). Figures (2) to (5) show iso-surfaces of the 36 kernels corresponding to density perturbations. They are plotted for values of $\pm s\cdot[(600\,\mathrm{km})^2\cdot(4\pi\rho c_{pq}^3)\cdot(4\pi\rho c_n^2)]^{-1}$, where the scaling factor s is given in the sub-figure titles. The velocity c_{pq} is $\alpha = 5\,\mathrm{km\,s^{-1}}$ for the P→Y kernels and $\beta = 5/\sqrt{2}\,\mathrm{km\,s^{-1}}$ for the S→Y kernels. Similarly, c_n is α for the X→P kernels and β for the X→S kernels. Source and receiver are located at $(x, y, z) = (200, 500, 500)\,\mathrm{km}$ and $(x, y, z,) = (800, 500, 500)\,\mathrm{km}$, respectively. Black lines intersecting at the source indicate the directions p and q.
Despite the simplicity of the problem, the sensitivity densities reveal a considerable

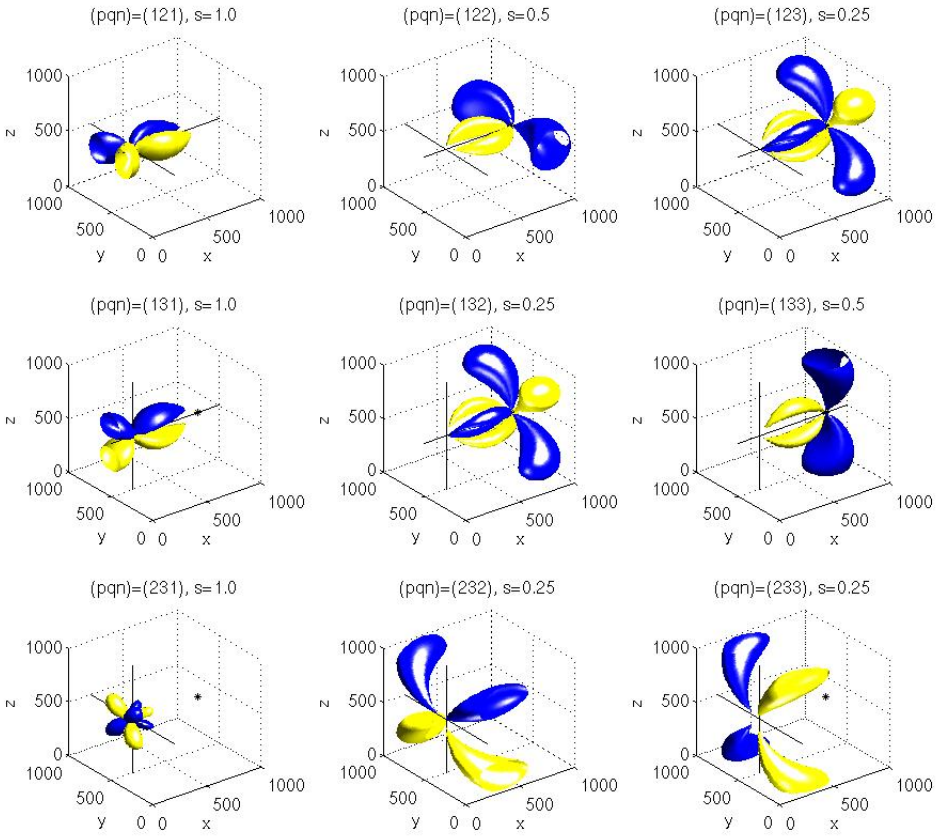

Fig. 2. Iso-surfaces of the sensitivity kernels $-\mathbf{a}_{pq}^{PFF} \cdot \mathbf{b}_{n}^{PFF}$ plotted at values of $\pm s \cdot [(600\,\mathrm{km})^2 \cdot (4\pi\rho\alpha^3) \cdot (4\pi\rho\alpha^2)]^{-1}$, where the scaling factor s is given in the sub-figure titles. Yellow denotes positive and blue negative values. Wave speeds are $\alpha = 5\,\mathrm{km\,s^{-1}}$ and $\beta = \alpha/\sqrt{2}\,\mathrm{km\,s^{-1}}$. The source is located at $(x, y, z) = (200, 500, 500)\,\mathrm{km}$ and the receiver, marked by a star (*), is at $(x, y, z) = (800, 500, 500)\,\mathrm{km}$. Black lines intersecting at the source indicate the (pq)-plane. The index n represents the observation direction. The sensitivity kernels plotted in the first row ($(1, 2)$-couple) have expected correspondences in the second row ($(1, 3)$-couple). It is noteworthy that there are significant sensitivity contributions between source and receiver only if one of the two source dipoles points towards the receiver. Therefore, in the case of the $(2, 3)$-couple the sensitivities practically vanish in the region between source and receiver. Large sensitivity contributions in regions behind source or receiver and far away from the line connecting source and receiver arise if the observation direction n does not point toward the source.

complexity. As expected, they depend on both the observation direction n and the source orientation (pq). In general, all the sensitivity densities are small along the line connecting source and receiver. This has important consequences: Assume that we observe a waveform difference in the direct wave (either P or S) that is due to a density perturbation. (Of course, in practice we may not know the character of the perturbation. This is a gedanken experiment.) Then we know that this density

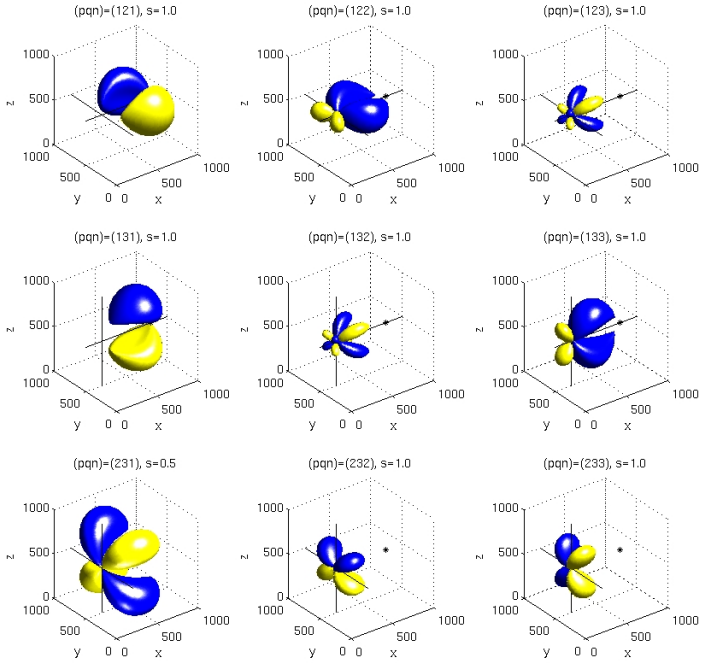

Fig. 3. The same as figure 2 but for the sensitivity kernels $-\mathbf{a}_{pq}^{PFF} \cdot \mathbf{b}_{n}^{SFF}$ (P to S conversions) plotted at values of $\pm s \cdot [(600\,\mathrm{km})^2 \cdot (4\pi\rho\alpha^3) \cdot (4\pi\rho\beta^2)]^{-1}$. The scaling factor s is given in the sub-figure titles. Symmetries between the first row ($(1,2)$-couple) and the second row ($(1,3)$-couple) are again due to choosing the line connecting source and receiver as parallel to the x-direction. In general the sensitivity densities are small near the region between source and receiver. This effect is especially pronounced in the case of the $(2,3)$-couple, as already observed for the P→P kernels shown in figure 2.

perturbation must be located somewhere along the line (or more generally the ray) connecting source and receiver. If it were not located on that line, the secondary wave emanating from that density perturbation would arrive later and therefore not translate to a waveform change of the direct wave, at least if its temporal bandwidth is sufficiently short. However, the sensitivity kernels for density perturbations are small or even zero on that line. But there are two exceptions, namely the source and the receiver regions where all sensitivity kernels have a singularity. Thus, we can conclude that the density perturbation is very likely to be located near the source or receiver because if it were located somewhere else along the source-receiver line, it would have to have a very large and probably unrealistic amplitude. Consequently, one may want to exclude direct waves from a waveform inversion because the corresponding residuals will map almost exclusively into the source and receiver regions. Alternatively, one could use the direct wave but at the same time exclude the source and receiver regions from the inversion by setting the derivatives there to zero.

Another important aspect of figures 2 to 5 is their scaling. The values of the P→P kernels are proportional to $\alpha^{-3}\alpha^{-2}$, whereas the other kernels have values propor-

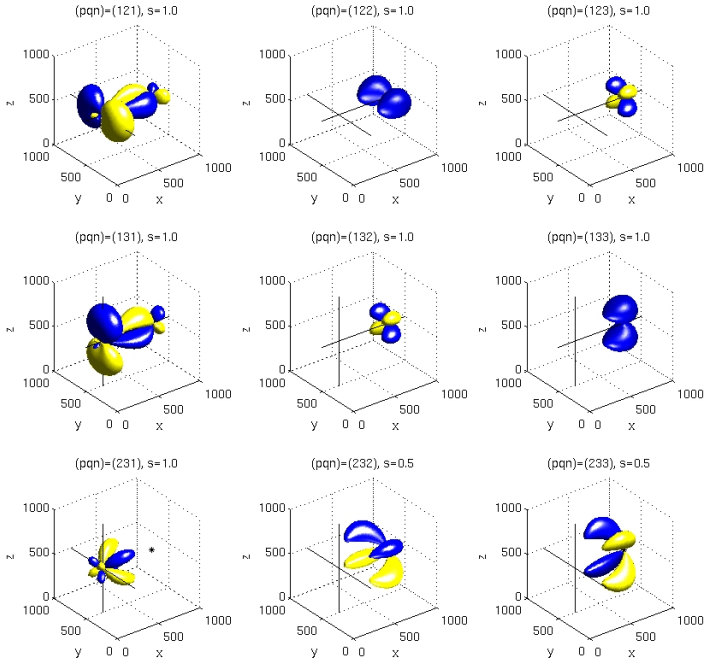

Fig. 4. The same as figure 2 but for the sensitivity kernels $-\mathbf{a}_{pq}^{SFF} \cdot \mathbf{b}_{n}^{PFF}$ (S to P conversions) plotted at values of $\pm s \cdot [(600\,\mathrm{km})^2 \cdot (4\pi\rho\beta^3) \cdot (4\pi\rho\alpha^2)]^{-1}$. The scaling factor s is given in the sub-figure titles. As expected from the source-receiver asymmetry of the sensitivity kernels, there are no similarities between the S→P kernels and the P→S kernels shown in figure 3. Generally, the sensitivity densities are small in the region between source and receiver, the only exceptions being the (121) and the (131) kernel.

tional to $\alpha^{-3}\beta^{-2}$ (P→S), $\beta^{-3}\alpha^{-2}$ (S→P) and $\beta^{-3}\beta^{-2}$ (S→S), respectively. The implication for any waveform inversion is that S-wave residuals dominate and that P-wave residuals are suppressed, therefore potentially leading to an unbalanced exploitation of information contained in a seismogram. Waveform residuals due to a perturbation in λ will be comparatively small because they are pure P-wave residuals.

In figure 2 we observe that the $(1,2)$-double couples correspond to kernels for the $(1,3)$-double couples with different observation directions. This symmetry arises from choosing the source-receiver line parallel to the x-direction. Similar correspondences can be found for the P→S, S→P and S→S kernels. Since the sensitivity kernels for density are just a product of the radiation pattern of the source double couple and the radiation pattern of a single force pointing in the observation direction, they can directly be interpreted in terms of these patterns. The (121)-kernels in figures 2 and 3 must vanish on the source-receiver line because the P-wave amplitude along this line is zero.

Similar arguments can be found for the S→P kernels in figure 4. The $(1,2)$- and $(1,3)$-double couples do generate S-wave motion between source and receiver. However, a P-wave set off by an S-wave incident on a density perturbation lo-

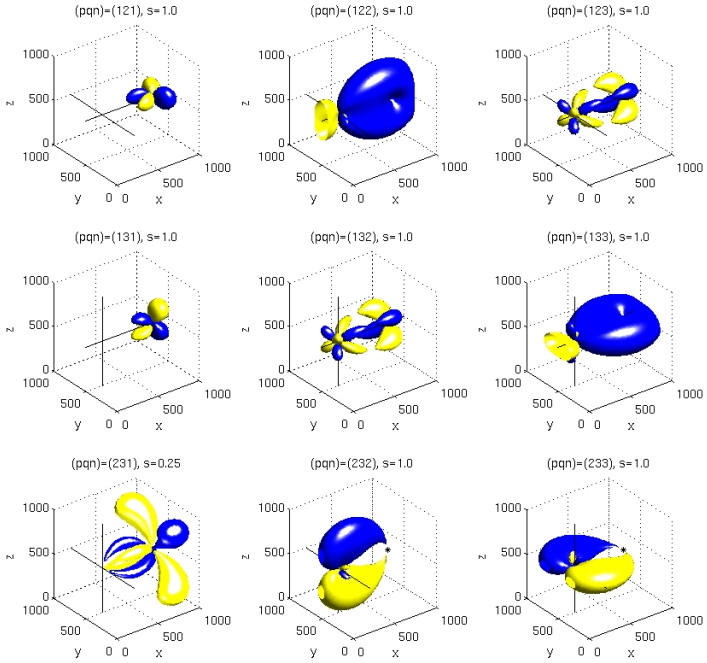

Fig. 5. The same as figure 2 but for the sensitivity kernels $-\mathbf{a}_{pq}^{SFF} \cdot \mathbf{b}_{n}^{SFF}$ plotted at values of $\pm s \cdot [(600\,\mathrm{km})^2 \cdot (4\pi\rho\beta^3) \cdot (4\pi\rho\beta^2)]^{-1}$. The scaling factor s is given in the sub-figure titles. Again, most of the sensitivity densities are concentrated in regions around source or receiver. Significant contributions along the line connecting source and receiver can only be observed in the cases of the (122) and (133) kernels.

cated somewhere on the source-receiver line, has zero amplitude along that line. This is because the incident S-wave acts as a single force in the y- or z-direction, respectively.

Generally, the sensitivity kernels corresponding to λ and μ do not allow such simple interpretations because they are the products of more complicated patterns.

At this point one may conclude that one general feature of the density sensitivity kernels involving S-waves (primary or secondary) is that they are collectively small or even zero between source and receiver. So far however, we considered only very specific geometries, namely those where the dipole directions coincide with the coordinate directions. A different set up is presented in figure 6 for the case of P→S kernels. The source-receiver line has been rotated by 45^o, so that the source is now located at $(x, y, z) = (300, 300, 500)$ km and the receiver is at $(x, y, z) = (724, 724, 500)$ km. Despite this modification, the P→S kernels shown in figure 6 do not differ much from those presented in figure 3. Only the size of the lobes changes and they are curved towards either source or receiver. The general feature, namely the fact that they vanish in the region between source and receiver, remains.

Finally, we consider the sensitivity kernels corresponding to the parameters μ and λ. A perturbation in μ is expected to set off both a secondary S- and a secondary

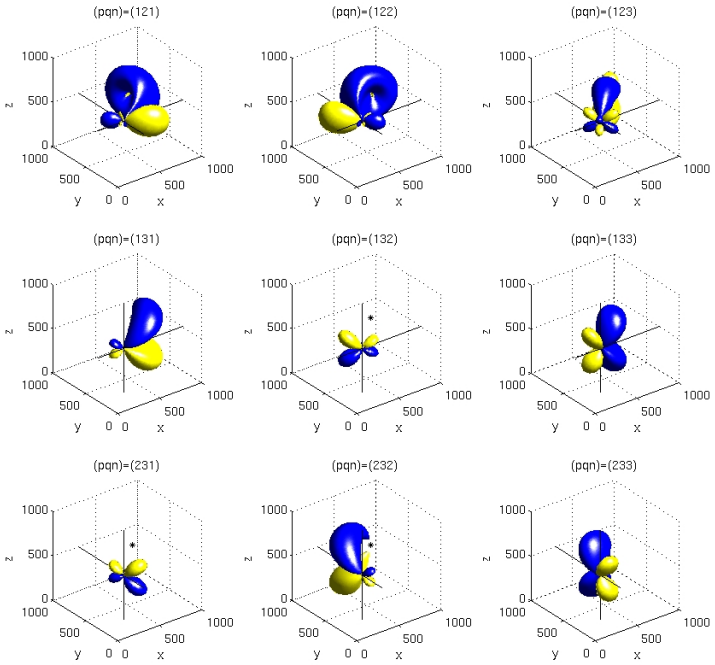

Fig. 6. The same as figure 3 but with the source and the receiver located at $(x, y, z) = (300, 300, 500)$ km and $(x, y, z) = (724, 724, 500)$ km, respectively. Symmetries between the first row ($(1, 2)$-couple) and the second row ($(1, 3)$-couple) as observed in figure 3 do not exist. In general the sensitivity densities are small in the region between source and receiver. This effect is again especially pronounced in the case of the $(2, 3)$-couple.

P-wave. In particular we find that the far field sensitivity kernels for μ are given by

$$M_{pqn}^{X\to Y} = -\mathbf{A}_{pq}^{XFF} : \mathbf{B}_{n}^{YFF} - \mathbf{A}_{pq}^{XFF} : \left(\mathbf{B}_{n}^{YFF}\right)^{T} , \tag{53}$$

where X and Y denote either S or P. It is demonstrated in the appendix that the cartesian components of the second-order tensors $\mathbf{A}_{pq}^{XFF}$ and $\mathbf{B}_{n}^{YFF}$ are

$$\begin{aligned}
\left(\mathbf{A}_{pq}^{PFF}\right)_{ij} &= \frac{\gamma_p^{(s)}\gamma_q^{(s)}\gamma_i^{(s)}\gamma_j^{(s)}}{4\pi\rho\alpha^4 r^{(s)}} & \left(\mathbf{A}_{pq}^{SFF}\right)_{ij} &= \frac{\gamma_q^{(s)}\gamma_i^{(s)}}{4\pi\rho\beta^4 r^{(s)}}\left(\delta_{jp} - \gamma_j^{(s)}\gamma_p^{(s)}\right) , \\
\left(\mathbf{B}_{n}^{PFF}\right)_{ij} &= \frac{\gamma_j^{(r)}\gamma_i^{(r)}\gamma_n^{(r)}}{4\pi\rho\alpha^3 r^{(r)}} , & \left(\mathbf{B}_{n}^{SFF}\right)_{ij} &= \frac{\gamma_i^{(r)}}{4\pi\rho\beta^3 r^{(r)}}\left(\delta_{jn} - \gamma_j^{(r)}\gamma_n^{(r)}\right) .
\end{aligned} \tag{54}$$

It is not possible to interpret these kernels simply in terms of multiplied radiation patterns. Their maximum values are a factor of $\alpha^{-1}\beta^{-1}$ smaller than the maximum values of the sensitivity kernels for density.

From equation (45d) we see that a perturbation in λ will not create any secondary far field S-waves because the divergence of the adjoint S-wave Green's function

has no far field contribution. Since the same is true for the original S-wave Green's function, there is only one sensitivity kernel for λ for the different double couple orientations and observation directions:

$$L^{FF}_{pqn} := -a^{FF}_{pq} b^{FF}_{n} \, . \tag{55}$$

The scalars a^{FF}_{pq} and b^{FF}_{n} are given by

$$a^{FF}_{pq} = \frac{\gamma^{(s)}_p \gamma^{(s)}_q}{4\pi\rho\alpha^4 r^{(s)}} \, , \qquad b^{FF}_{n} = \frac{\gamma^{(r)}_n}{4\pi\rho\alpha^3 r^{(r)}} \, . \tag{56}$$

See the appendix for a detailed derivation. The general characteristics of the sensitivity kernels for density translate to the kernels for μ and λ. In particular, they are small in the region between source and receiver.

5 Discussion

The sensitivity $\mathbf{s}$ is defined as the first derivative of an observable $\mathbf{u}(\mathbf{p})$ with respect to the model parameters $\mathbf{p}$. It can be expressed by the Green's functions of the original and the adjoint problem (e.g. Tarantola, 1984, 1988; Talagrand & Courtier, 1987; Sun, 1994; Bunge et al., 2003). An analysis for the case of the acoustic wave equation $p\,\partial_t^2 u - \Delta u = f$ led to the result that the sensitivity $s(\boldsymbol{\xi}_0, \tau_0)$ vanishes for times τ_0 that are smaller than the arrival time of the first wavefront at the observation point $\boldsymbol{\xi}_0$. This is true for all possible differentiation directions (perturbations) $\delta p(\mathbf{x})$ and in particular for those that would lead to earlier arrivals. Information about traveltime anomalies must therefore be contained in higher derivatives of the wavefield.

This characteristic influences the total derivative of an objective function $\mathfrak{E}$ with respect to $\mathbf{p}$ through equation (12). When $\mathfrak{E}$ is chosen to be the least squares objective function defined in equation (37) then $D_p\mathfrak{E}$ only detects the edges of a perturbation if the signal wavelength is too short. The interior of the perturbation remains 'invisible' (Gauthier et al. 1986). However, choosing the signal wavelength several times longer than the dimension of the perturbation, causes the perturbation to act as a diffractor and therefore it maps into the derivative as one single but relatively broad peak. It can be concluded that such a waveform inversion relies on a sufficiently precise background model in order to guarantee that the remaining parameter differences between the true Earth model and the numerical model merely act as scatterers. The background model can be obtained by a conventional traveltime tomography. Alternatively one could start with very long wavelengths which then successively decrease in the course of the waveform inversion.

The extent to which the lack of traveltime information in the sensitivity maps to the properties of the derivative of an objective function $\mathfrak{E}$ depends on the definition of $\mathfrak{E}$ itself. Luo & Schuster (1991) explicitly introduced traveltime differences into

the objective function. Their approach overcomes the problem that only the edges of perturbations are detected but it also results in a lower resolution.
Pratt et al. (1998) proposed to use also the second derivative of the least squares objective function to solve the minimisation problem. They demonstrated that $D_p\mathfrak{E}$ multiplied by the inverse Hessian images a perturbation better than $D_p\mathfrak{E}$ alone. However, the calculation and inversion of the second derivative is computationally too expensive for sufficiently realistic Earth models.
The problem of missing traveltime information could alternatively be circumvented by using Monte Carlo methods in order to minimise the objective function. This approach relies on the evaluation of a large number of parameter space elements $\mathbf{p} \in P$ and it therefore becomes impractical if the solution of the forward problem is as time consuming as it is in seismology.
It is important to note that sensitivities and first derivatives in general are physically meaningful only if the problem is either linear or if it can be reasonably linearized. The latter requires that the reference model be sufficiently close to the true model so that parameter differences only act as scatterers. If significant non-linearities remain, the first derivatives of $\mathfrak{E}$ and $\mathbf{u}$ only bear insufficient information.
Dipolar sources are of particular interest in seismology because they allow us to represent the sources of most tectonic earthquakes observed at great distances from the source region. By considering the elastic wave equation in an unbounded homogeneous medium we found that the sensitivity kernels for each parameter (density ρ and the two Lamé parameters μ and λ), decompose into four summands to which we referred as P→P, P→S, S→P and S→S kernels. The X→Y kernels, where X and Y are either P or S, may be interpreted in terms of secondary Y-waves set off by a primary X-wave incident on a parameter perturbation. Generally, the sensitivity kernels can be represented by a product of two factors. In the case of the sensitivity kernels for density, the two factors correspond to the radiation patterns of the forward field and the adjoint field, respectively. The factors involved in the sensitivity kernels for λ and μ are more complex than the normal radiation patterns of elastic waves.
All sensitivity kernels exhibit singularities at the source and receiver and are small in the region between them. This together with the fact that the first derivative only accounts for scattering implies that waveform residuals of the direct waves (P or S) will almost exclusively map into the source and receiver regions. Therefore one should exclude either the direct waves or the source and receiver regions from the inversion procedure.
Some of the sensitivity kernels are almost restricted to regions behind the source or receiver. Consequently, one may wish to exclude these unfavourable source-receiver configurations from the inversion. This requires information about both the source orientation and the waveform that one attempts to reconstruct. Good quality information about the source orientation is usually available. It is however practically impossible to identify a waveform residual as being due to a particular X→Y conversion arising from parameter differences between the true Earth model and the numerical model.
In the same context we also found that the S→S kernel is larger than the S→P and

P→S kernels, which in turn are larger than the P→P kernels. Since this is true for any parameter perturbation, with the exception of perturbations in λ which do not involve S-waves, we conclude that waveform changes corresponding to the S kernels dominate those corresponding to the pure P kernels. This implies that S-wave residuals, i.e., residuals with zero divergence, will dominate the misfit functional or objective function. The implications of such an unbalanced use of waveform information on the actual inversion outcome certainly need further investigation. Generally it can be expected that variations in λ will be more difficult to detect than variations in μ or ρ because they do not generate S-waves. One may correct for this effect of S-wave dominance by including measurements of rotational motion that allow to separate P- and S-wave motion (e.g. Nigbor, 1994; Pancha et al., 2000; Igel et al., 2005). Alternatively, one could only consider the waveform of the direct P wave, therefore minimising the influence of S-waves. This would unfortunately eliminate the major advantage of waveform inversion, namely the possibility of accounting for a maximum of information contained in a seismogram.

Most of the results obtained in the course of this study are based on very simple models that are not realistic. But still, since the deduced phenomena have fundamental character one can assume that they will also be present in more complicated scenarios.

An adjoint method based waveform inversion should also be viewed in the context of seismic inversions based on ray theory and truncated normal mode expansions (e.g. Masters et al., 1996; Grand, 1997; Mégnin & Romanowicz, 2000; Kennett & Gorbatov, 2004). Seismic imaging based on ray theory relies on a dense sampling of the regions of interest because ray traveltime sensitivities are in theory spatially restricted to the ray. Therefore, a localised traveltime anomaly will not be visible if there is no ray that penetrates it. However, sensitivity off the ray path can be artificially introduced through a parametrization of the model with sufficiently extended basis functions and through regularization. This produces smoothed inhomogeneities that may influence ray paths that are unaffected by a rough and spatially less extended inhomogeneity. Normal modes map local effects into global ones. This is an advantage because the normal mode waveforms, obtained by a finite summation over global basis functions contain information about every point inside the Earth. This, however, affects the resolution negatively. If based on the adjoint method, waveform inversion is in that sense between the two extremes of ray theory and normal modes. Depending on the particular sensitivity distribution, a parameter perturbation can be observed even if there is no ray passing through it. But still, this parameter perturbation will not have a global effect as it would if the synthetic seismograms were computed via a truncated normal mode expansion. The fact that the first derivative of the observed wavefield with respect to the parameters does not account for traveltime differences determines the possible applications of an adjoint method based waveform inversion. It may for example be used to determine the sharpness of discontinuities such as those caused by phase transitions in the Earth's mantle. Other regions where such a waveform inversion may be useful include the thermal boundary layers, i.e., the crust and D", where one may expect more short wavelength heterogeneity than in the remaining mantle.

6 Conclusions

Departing from the definition of sensitivity functionals that allow us to express the sensitivity in terms of Green's functions, we found that the first derivative of an observed wavefield with respect to the model parameters does not account for traveltime differences. The direct consequence is that a gradient-method based waveform inversion relies on an accurate background model. This background model may either be obtained through a conventional traveltime inversion or by using longer wavelengths. In the case of elastic wavefields set off by dipolar sources we saw that the surprisingly complex shape of waveform sensitivity kernels depends strongly on both the source orientation and the observation direction. The fact that most kernels vanish in the region between source and receiver implies that one should exclude either the direct waves or the source and receiver regions from a waveform inversion. The effect of S-wave residual dominance may significantly affect the inversion outcome, therefore posing the problem of exactly characterising different wave types in a seismogram. This may in the future be accomplished by including rotational measurements that allow a separation of P- and S-wave motion. Possible applications of the adjoint method in the context of waveform inversion include the imaging of smaller scale structures that act as scatterers and which cannot be resolved by ray tomography or inversions based on truncated normal mode expansions. Moreover, it may be possible to determine the sharpness of discontinuities with increased accuracy.

Acknowledgements

The authors wish to thank Brian Kennett, Bernhard Forkmann and Steve Haney for discussions and constructive criticism.

References

[1] Aki, K. & P. G. Richards, 2002. *Quantitative Seismology*, 2nd edn., University Science Books.

[2] Bunge, H.-P., C. R. Hagelberg, B. J. Travis, 2003. Mantle circulation models with variational data assimilation: inferring past mantle flow and structure from plate motion histories and seismic tomography, *Geophys. J. Int.*, **152**, 280-301.

[3] Cichowicz, R. W. E. Green, 1992. Tomographic study of upper-mantle structure of the South African continent, using wave-form inversion, *Phys. Earth planet. Int.*, **72**, 276-285.

[4] Crase, I., Pica, A., Noble, M., McDonald, J., Tarantola, A., 1990. Robust elastic nonlinear waveform inversion: Application to real data, *Geophysics*, **55**(5), 527-538.

[5] Dziewonski, A. M., D. L. Anderson, 1981. Preliminary reference Earth model, *Phys. Earth Planet. Int.*, **25**, 297-356.

[6] Dziewonski, A. M., 1984. Mapping the lower mantle: Determination of lateral

heterogeneity in P-velocity up to degree and order 6, *J. Geophys. Res.*, **89**, 5929-5952.

[7] Fichtner, A., H.-P. Bunge, H. Igel, 2005. The adjoint method in seismology – I. Theory, submitted.

[8] Gauthier, O., J. Virieux, A. Tarantola, 1986. Two-dimensional nonlinear inversion of seismic waveforms: Numerical results, *Geophysics*, **51**, No. 7, 1387-1403.

[9] Grand, S. P., 1994. Mantle shear structure beneath the Americas and surrounding oceans, *J. Geophys. Res.*, **99**, 11,591-11,621.

[10] Grand, S., R. D. van der Hilst, S. Widiyantoro, 1997. Global seismic tomography: A snapshot of convection in the Earth, *GSA Today*, **7**, n. 4, 1-7.

[11] Igel, H., P. Mora, B. Riollet, 1995. Anisotropic wave propagation through finite-difference grids, *Geophysics*, **60**(4), 1203-1216.

[12] Igel, H., H. Djikpéssé, A. Tarantola, 1996. Waveform inversion of marine reflection seismograms for P impedance and Poisson's ratio, *Geophys. J. Int.*, **124**(2), 363-371.

[13] Igel, H., U. Schreiber, A. Flaws, B. Schuberth, A. Velikoseltsev, A. Cochard, 2005. Rotational motions induced by the M8.1 Tokachi-oki earthquake, September 25, 2003, *Geophys. Res. Lett.*, **32**, L08309, doi:10.1029/2004GL022336.

[14] Kennett, B. L. N., E. R. Engdahl, 1991. Traveltimes for global earthquake location and phase identification, *Geophys. J. Int.*, **105**, 429-465.

[15] Kennett, B. L. N., E. R. Engdahl, R. Buland, 1995. Constraints on seismic velocities in the Earth from traveltimes, *Geophys. J. Int.*, **122**, 108-124.

[16] Kennett, B. L. N., A. Gorbatov, 2004. Seismic heterogeneity in the mantle - strong shear wave signature of slabs from joint tomography, *Phys. Earth Planet. Int.*, **146**, 87-100.

[17] Komatitsch, D., C. Barnes, J. Tromp, 2000. Simulation of anisotropic wave propagation based upon a spectral element method, *Geophysics*, **65**(4), 1251-1260.

[18] Li, X.-D., T. Tanimoto, 1993. Waveforms of long-period body waves in a slightly aspherical Earth model, *Geophys. J. Int.*, **112**, 92-102.

[19] Li, X.-D., B. Romanowicz, 1995. Comparison of global waveform inversions with and without considering cross-branch modal coupling, *Geophys. J. Int.*, **121**, 695-709.

[20] Luo, Y., G. T. Schuster, 1991. Wave-equation traveltime inversion, *Geophysics*, **56**(5), 645-653.

[21] Marquering, H., R. Snieder, G. Nolet, 1996. Waveform inversions and the significance of surface-wave mode coupling, *Geophys. J. Int.*, **124**, 258-278.

[22] Masters, G., S. Johnson, G. Laske, H. Bolton, 1996. A shear-velocity model of the mantle, *Phil. Trans. R. Soc. Lond., A*, **354**, 1385-1411.

[23] Mégnin, C., B. Romanowicz, 2000. The three-dimensional shear velocity structure of the mantle from the inversion of body, surface and higher-mode waveforms, *Geophys. J. Int.*, **143**, 709-728.

[24] Nigbor, R., 1994. Six-degrees-of-freedom ground-motion measurement, *Bull. Seismol. Soc. Am.*, **84**, 1665-1669.

[25] Pancha, A., T. H. Webb, G. E. Stedman, D. P. McLeod, U. Schreiber, 2000. Ring laser detection of rotatitions from teleseismic waves, *Geophys. Res. Lett.*, **27**, 3553-3556.

[26] Pratt, R. G., C. Shin, G. J. Hicks, 1998. Gauss-Newton and full Newton methods in frequency-space seismic waveform inversion, *Geophys. J. Int.*, **133**, 341-362.

[27] Sun, N.-Z., 1994. *Inverse problems in groundwater modelling*, Kluwer Academic Publishers.

[28] Talagrand, O., P. Courtier, 1987. Variational assimilation of meteorological observations with the adjoint vorticity equation. I: Theory, *Q. J. R. Meteorol. Soc.*, **113**, 1311-1328.

[29] Tarantola, A., 1984. Inversion of seismic reflection data in the acoustic approximation, *Geophysics*, **49**, No. 8, 1259-1266.

[30] Tarantola, A., 1987. *Inverse problem theory. Methods for data fitting and model parameter estimation.*, Elsevier, Amsterdam.

[31] Tarantola, A., 1988. Theoretical background for the inversion of seismic waveforms, including elasticity and attenuation, *Pure and Appl. Geophys.*, **128**, 365-399.

[32] Tromp, J., C. Tape, Q. Liu, 2005. Seismic tomography, adjoint methods, time reversal, and banana-donut kernels, *Geophys. J. Int.*, **160**, 195-216.

[33] Zielhuis, A., R. D. van der Hilst, 1996. Upper-mantle shear velocity beneath eastern Australia from inversion of waveforms from SKIPPY portable arrays, *Geophys. J. Int.*, **127**, 1-16.

A Sensitivity kernels

We begin with the derivation of the sensitivity kernels for density. The kernels corresponding to the parameters λ and μ can be derived in a similar way. Inserting the expressions of Green's functions in equations (46) and (47) into the density sensitivity functional given in equation (45b) yields

$$S^{\rho}_{pqn}(\boldsymbol{\xi}_0, \tau_0; h, \rho') = \int_{-\infty}^{\infty} \int_{t=t_0}^{t_1} \int_{\mathbb{R}^3} \sum_{X,Y} \rho' \, \mathbf{a}^{XFF}_{pq} \cdot \mathbf{b}^{YFF}_{n} \, \ddot{\delta}\left(t - \tau - t_0 - r^{(s)}/c_X\right) \dot{\delta}\left(r^{(r)}/c_Y + t - \tau_0\right) \, h(\tau) \, d\tau \, dt \, d^3\mathbf{x} \,, \quad \text{(A.1)}$$

where the summation $\sum_{X,Y}$ is over the four possible combinations of $X = P, S$ and $Y = P, S$. Moreover, $c_P = \alpha$ and $c_S = \beta$. The vectors $\mathbf{a}^{XFF}_{pq}$ and $\mathbf{b}^{YFF}_{n}$ are

defined by

$$\mathbf{a}_{pq}^{PFF} = \frac{\gamma_p^{(s)}\gamma_q^{(s)}}{4\pi\rho\alpha^3 r^{(s)}}\frac{\mathbf{r}^{(s)}}{r^{(s)}}\,, \qquad \mathbf{a}_{pq}^{SFF} = \frac{\gamma_q^{(s)}}{4\pi\rho\beta^3 r^{(s)}}\left(\mathbf{e}_p - \frac{\mathbf{r}^{(s)}}{r^{(s)}}\gamma_p^{(s)}\right)\,,$$
$$\mathbf{b}_{n}^{PFF} = \frac{\gamma_n^{(r)}}{4\pi\rho\alpha^2 r^{(r)}}\frac{\mathbf{r}^{(r)}}{r^{(r)}}\,, \qquad \mathbf{b}_{n}^{SFF} = \frac{1}{4\pi\rho\beta^2 r^{(r)}}\left(\mathbf{e}_n - \frac{\mathbf{r}^{(r)}}{r^{(r)}}\gamma_n^{(r)}\right)\,. \tag{A.2}$$

Integration with respect to τ gives

$$S_{pqn}^{\rho}(\boldsymbol{\xi}_0,\tau_0;h,\rho') = \int_{t=t_0}^{t_1}\int_{\mathbb{R}^3}\sum_{X,Y}\rho'\,\mathbf{a}_{pq}^{XFF}\cdot\mathbf{b}_{n}^{YFF}\,\ddot{h}\left(t-t_0-r^{(s)}/c_X\right) \dot{\delta}\left(r^{(r)}/c_Y + t - \tau_0\right)\,dt\,d^3\mathbf{x}\,. \tag{A.3}$$

The remaining integral is non-zero only if the observation time τ_0 satisfies the condition

$$\tau_0 \in (t_0 + r^{(r)}/c_Y, t_1 + r^{(r)}/c_Y)\,. \tag{A.4}$$

Note that we also require $\tau_0 \in [t_0, t_1]$ which means that the observation time must be in the observation interval. Assuming that (A.4) is satisfied, we obtain

$$S_{pqn}^{\rho}(\boldsymbol{\xi}_0,\tau_0;h,\rho') = -\int_{\mathbb{R}^3}\sum_{X,Y}\rho'\,\mathbf{a}_{pq}^{XFF}\cdot\mathbf{b}_{n}^{YFF}\,\dddot{h}\left(\tau_0 - t_0 - r^{(s)}/c_X - r^{(r)}/c_Y\right)\,d^3\mathbf{x}\,. \tag{A.5}$$

The causality of the source time function h implies that S_{pqn}^{ρ} is non-zero only if

$$\tau_0 \geq t_0 + r^{(s)}/c_X + r^{(r)}/c_Y\,. \tag{A.6}$$

The integrations in the case of the sensitivity functional for μ are identical to those outlined for the density sensitivity functional. It therefore suffices to derive the kernels themselves. For the gradients of the different Green's functions we find

$$\nabla\mathbf{g}_{pq}^{PFF}(\mathbf{x}_0,t_0;\mathbf{x},t) \overset{FF}{=} -\mathbf{A}_{pq}^{PFF}\,\ddot{\delta}(t-t_0-r^{(s)}/\alpha)\,, \tag{A.7a}$$
$$\nabla\mathbf{g}_{pq}^{SFF}(\mathbf{x}_0,t_0;\mathbf{x},t) \overset{FF}{=} -\mathbf{A}_{pq}^{SFF}\,\ddot{\delta}(t-t_0-r^{(s)}/\beta)\,, \tag{A.7b}$$
$$\nabla\mathbf{g}_{n}^{*PFF}(\mathbf{x}_0,\tau_0;\mathbf{x},t) \overset{FF}{=} \mathbf{B}_{n}^{PFF}\,\dot{\delta}(r^{(r)}/\alpha+t-\tau_0)\,, \tag{A.7c}$$
$$\nabla\mathbf{g}_{n}^{*SFF}(\mathbf{x}_0,\tau_0;\mathbf{x},t) \overset{FF}{=} \mathbf{B}_{n}^{SFF}\,\dot{\delta}(r^{(r)}/\beta+t-\tau_0)\,, \tag{A.7d}$$

where FF indicates that all near field terms generated through the differentiation have been neglected. The cartesian components of the second-order tensors $\mathbf{A}_{pq}^{XFF}$ and $\mathbf{B}_{n}^{YFF}$ are given by

$$\left(\mathbf{A}_{pq}^{PFF}\right)_{ij} = \frac{\gamma_p^{(s)}\gamma_q^{(s)}\gamma_i^{(s)}\gamma_j^{(s)}}{4\pi\rho\alpha^4 r^{(s)}}\,, \qquad \left(\mathbf{A}_{pq}^{SFF}\right)_{ij} = \frac{\gamma_q^{(s)}\gamma_i^{(s)}}{4\pi\rho\beta^4 r^{(s)}}\left(\delta_{jp}-\gamma_j^{(s)}\gamma_p^{(s)}\right)\,,$$
$$\left(\mathbf{B}_{n}^{PFF}\right)_{ij} = \frac{\gamma_j^{(r)}\gamma_i^{(r)}\gamma_n^{(r)}}{4\pi\rho\alpha^3 r^{(r)}}\,, \qquad \left(\mathbf{B}_{n}^{SFF}\right)_{ij} = \frac{\gamma_i^{(r)}}{4\pi\rho\beta^3 r^{(r)}}\left(\delta_{jn}-\gamma_j^{(r)}\gamma_n^{(r)}\right)\,. \tag{A.8}$$

These tensors must be multiplied according to equations (45e) and (53) in order to give the sensitivity kernels. The sensitivity functional for λ is substantially simpler than the ones for ρ and μ due to the fact that the divergence of all S-wave Green's functions has no far field component. For the P-wave Green's functions we find

$$\nabla \cdot \mathbf{g}_{pq}^{PFF}(\mathbf{x}_0, t_0; \mathbf{x}, t) \overset{FF}{=} -a_{pq}^{FF}\, \ddot{\delta}(t - t_0 - r^{(s)}/\alpha)\,, \tag{A.9a}$$

$$\nabla \cdot \mathbf{g}_{n}^{*\,PFF}(\mathbf{x}_0, \tau_0; \mathbf{x}, t) \overset{FF}{=} b_{n}^{FF}\, \dot{\delta}(r^{(r)}/\alpha + t - \tau_0)\,. \tag{A.9b}$$

The two scalars a_{pq}^{FF} and b_n^{FF} are

$$a_{pq}^{FF} = \frac{\gamma_p^{(s)}\gamma_q^{(s)}}{4\pi\rho\alpha^4 r^{(s)}}\,, \qquad b_n^{FF} = \frac{\gamma_n^{(r)}}{4\pi\rho\alpha^3 r^{(r)}}\,. \tag{A.10}$$